JOURNAL OF SYNCHROTRON RADIATION

ISSN 1600-5775

Received 6 November 2018
Accepted 22 April 2019

Edited by M. Yabashi, RIKEN SPring-8 Center, Japan

[1] This article will form part of a virtual special issue on X-ray free-electron lasers.

Keywords: free-electron lasers; hard X-rays; self-seeding; electron-energy jitter; diamond monochromators; self-amplified spontaneous emission.

Hard X-ray self-seeding commissioning at PAL-XFEL[1]

Chang-Ki Min,[a] Inhyuk Nam,[a]* Haeryong Yang,[a] Gyujin Kim,[a] Chi Hyun Shim,[a] Jun Ho Ko,[a] Myung-Hoon Cho,[a] Hoon Heo,[a] Bonggi Oh,[a] Young Jin Suh,[a] Min Jae Kim,[a] Donghyun Na,[a] Changbum Kim,[a] Yongsam Kim,[a] Sae Hwan Chun,[a] Jae Hyuk Lee,[a] Jangwoo Kim,[a] Sunam Kim,[a] Intae Eom,[a] Seung Nam Kim,[a] Tae-Yeong Koo,[a] Seungyu Rah,[a] Yuri Shvyd'ko,[b] Deming Shu,[b] Kwang-Je Kim,[b] Sergey Terentyev,[c] Vladimir Blank[c] and Heung-Sik Kang[a]

[a]Pohang Accelerator Laboratory, Pohang, Gyeongbuk 37673, Republic of Korea, [b]Argonne National Laboratory, Argonne, IL 60439-4815, USA, and [c]Technological Institute for Superhard and Novel Carbon Materials, Troitsk, Moscow 142190, Russian Federation. *Correspondence e-mail: ihnam@postech.ac.kr

A wake monochromator based on a large-area diamond single crystal for hard X-ray self-seeding has been successfully installed and commissioned in the hard X-ray free-electron laser (FEL) at the Pohang Accelerator Laboratory with international collaboration. For this commissioning, the self-seeding was demonstrated with a low bunch charge (40 pC) and the nominal bunch charge (180 pC) of self-amplified spontaneous emission (SASE) operation. The FEL pulse lengths were estimated as 7 fs and 29.5 fs, respectively. In both cases, the average spectral brightness increased by more than three times compared with the SASE mode. The self-seeding experiment was demonstrated for the first time using a crystal with a thickness of 30 μm, and a narrow bandwidth of 0.22 eV (full width at half-maximum) was obtained at 8.3 keV, which confirmed the functionality of a crystal with such a small thickness. In the nominal bunch-charge self-seeding experiment, the histogram of the intensity integrated over a 1 eV bandwidth showed a well defined Gaussian profile, which is evidence of the saturated FEL and a minimal electron-energy jitter ($\sim 1.2 \times 10^{-4}$) effect. The corresponding low photon-energy jitter ($\sim 2.4 \times 10^{-4}$) of the SASE FEL pulse, which is two times lower than the Pierce parameter, enabled the seeding power to be maximized by maintaining the spectral overlap between SASE FEL gain and the monochromator.

1. Introduction

A millijoule-level femtosecond tunable hard X-ray laser source is now available from large-scale free-electron laser (FEL) facilities with lengths of a few hundred metres to a few kilometres. The lasing process of all of the facilities is based on self-amplified spontaneous emission (SASE), in which the electron-bunch length is typically hundreds of times longer than the temporal coherence length in the nominal bunch-charge mode (150–250 pC) so that hundreds of separated longitudinal modes are present and fluctuate in single-shot spectra within the SASE bandwidth (generally, 0.2–0.4% of a photon energy) (Huang & Kim, 2007; Gutt *et al.*, 2012). Currently self-seeding is the only available method to generate a millijoule FEL X-ray pulse in a single longitudinal mode, in the absence of external seeding in this high photon-energy range. The initial idea of self-seeding was based on the utilization of Bragg diffraction (BD) from a four-bounce diamond-crystal monochromator as a bandpass filter (Saldin *et al.*, 2001). A transmission self-seeding with simple alignment

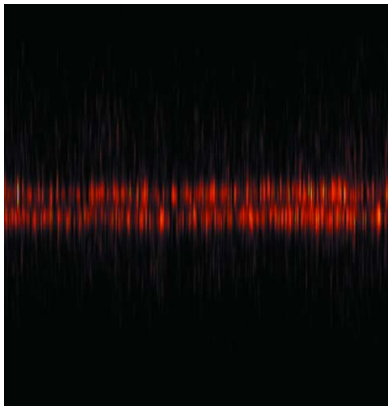

requirements was proposed using forward Bragg diffraction (FBD) from a single diamond crystal (Geloni *et al.*, 2011). The FBD diamond wake monochromator was used in the first demonstration of hard X-ray self-seeding at the Linac Coherent Light Source (LCLS) (Amann *et al.*, 2012).

The hard X-ray FEL at the Pohang Accelerator Laboratory (PAL-XFEL) was successfully commissioned in the SASE operation mode as the third hard X-ray FEL in 2016 (Kang *et al.*, 2017). In an effort to diversify its applications, the self-seeding based on the FBD monochromator was chosen. PAL collaborated with Argonne National Laboratory and the Technological Institute for Superhard and Novel Carbon Materials especially for designing the monochromator and manufacturing large-area defect-free diamond crystals and those characterizations of crystallinity. The monochromator was manufactured by a Korean company (Seinyung Vactron Co. Ltd, Bucheon, South Korea) based on the engineering design and was installed in February 2018. The monochromator accommodates two diamond single crystals in the [100] and [110] orientations to satisfy various optimization conditions (Yang & Shvyd'ko, 2013). To reduce the X-ray absorption and the FBD spectral width, one crystal in the [110] orientation is specially designed to a smaller thickness of 30 µm compared with 90–100 µm thicknesses of other crystals.

In this commissioning paper, we describe the installation and the crystal calibration process, self-seeding with both low and high bunch charges, and self-seeding with the ultrathin 30 µm crystal. The seeding performance can be limited by the electron-energy jitter, as shown in a previous report (Amann *et al.*, 2012). Our electron-energy jitter with a modern radio-frequency (RF) system was only ∼0.01%, which is one order of magnitude smaller than the SASE bandwidth. Therefore, the seeded FEL X-ray pulse energy was minimally affected by energy jitter. To demonstrate this, the experiments and the simulations using *SIMPLEX* code were compared at the high bunch charge.

2. Installation and calibration of FBD self-seeding monochromator

The schematic layout of the self-seeding instrumentation and photographs of the two sets of diamond double-crystal systems mounted on holders are shown in Fig. 1. The diamond wake monochromator is located after eight 5 m-long out-vacuum undulators with $K \simeq 1.87$ and is served by a bandpass filter with a delay time of tens of femtoseconds. The delayed seed with a narrow spectrum is further amplified using twelve undulators downstream. The additional undulator spaces are reserved to increase the seeding power and to obtain saturation at the higher photon energy. Two sets of the diamond double-crystals systems, with the (100) and (110) crystals having the same size, 4 mm × 5 mm, are each mounted on a separate holder. Each holder contains two diamond crystals in the [100] and [110] orientations, and, in one holder, a challenging 30 µm ultrathin crystal with the [110] orientation is mounted to reduce optical absorption and FBD seeding linewidth. The crystals are mounted on chemical vapor deposition (CVD) diamond bases for good heat dissipation using CVD diamond clamps and graphite levers. The spring constant of the graphite levers is optimized to minimize the residual stress in maintaining enough holding force. The quality of the crystals was confirmed by double-crystal X-ray topography. The mounting strain was less than 1.5 µrad root mean square (r.m.s.) in the 2 mm × 2 mm working area, which corresponds to less than 0.02 eV r.m.s. in most of the seeding conditions (Shvyd'ko *et al.*, 2017). Only the 30 µm ultrathin crystal required an annealing process at 920 K to remove residual stress from manufacturing, and became whitish due to

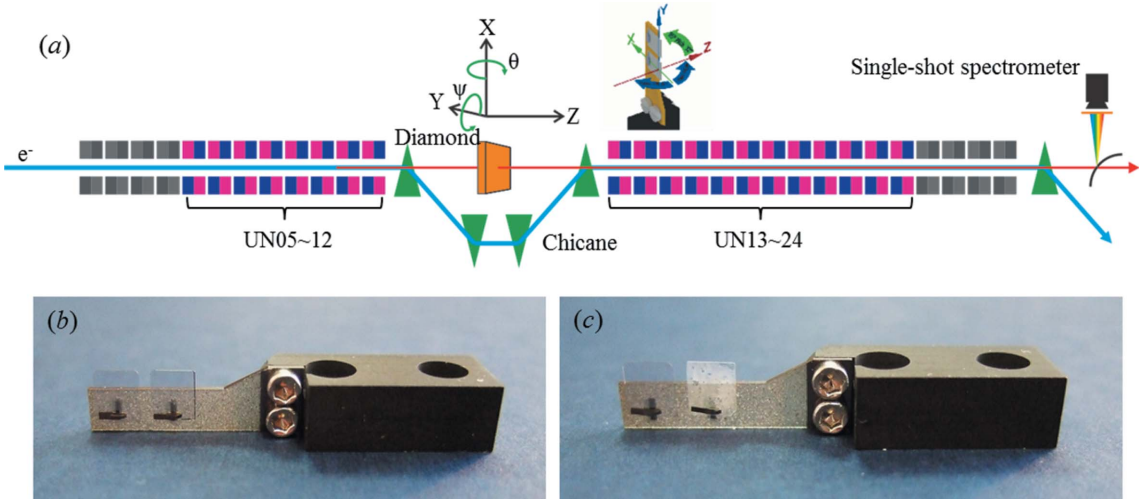

Figure 1
(*a*) Schematic layout of the self-seeding implementation at the hard X-ray undulator line of PAL-XFEL; 8 and 12 undulators are currently installed before and after the self-seeding system, respectively. The spaces for additional undulators in the future upgrade are shown in gray. The motion of the diamond crystal is automated for the angular motion of pitch (θ) and yaw (ψ), and for the translational motion of X and Y. (*b*, *c*) Photographs of two batches of crystals. (*b*) *C**[100] (left) and *C**[110] (right) crystals with thicknesses of 100 µm and 90 µm, respectively, were installed in the first batch. (*c*) *C**[100] (left) and *C**[110] (right) crystals with thicknesses of 100 µm and 30 µm, respectively, were installed in another batch. The 30 µm-thick crystal became foggy after the annealing process.

the roughen surface, which was not expected to degrade its crystallinity (Shvyd'ko *et al.*, 2017). The spectrum of the seeded FEL was measured by a Si(111) or Si(333) single-shot spectrometer (Zhu *et al.*, 2012). The low- and high-charge experiments were carried out using a Si(111) bent crystal with a spectral resolution of 0.6–0.8 eV. A recently installed Si(333) single-shot spectrometer with an improved resolution of 0.2 eV was used for the test with the 30 µm-thin crystal.

Fig. 2(*e*) shows a 3D drawing of the self-seeding section integrated onto the one-girder system. This monochromator system fits into one undulator as a modular design so that it can be replaced with any undulator in the future. The monochromator design is based on an LCLS mechanical drawing (Amann *et al.*, 2012) and was modified to accommodate a longer crystal holder with two crystals. The two rotation angles of the crystal were automated with the pitch angle θ in the range $32^\circ \leq \theta \leq 95^\circ$, and the yaw angle ψ in the range $-5.5^\circ \leq \psi \leq 4.4^\circ$. The beam propagation and the crystal plane are orthogonal when $\theta = 90^\circ$ and $\psi = 0^\circ$. The weak four-dipole chicane has a momentum compaction factor R_{56} in the range $5\ \mu\text{m} \leq R_{56} \leq 30\ \mu\text{m}$ for a delay time of 8–50 fs. Various diagnostic tools were implemented to monitor the position and size of the electron and photon beams and possible mechanical flaws: stripline beam-position monitor, in-line screen monitor, wire scanner, screen monitor for Bragg reflections and the surveillance camera. In the installation, the initial position and angle offsets of the crystals were checked with an aligned ultraviolet laser at 450 nm, which was visible in the screen monitor for Bragg reflections after a Be filter was detached. The piezo translational stage tended to induce a large deviation of about 1 mrad of reflected ultraviolet laser radiation due to vibration when moving, and the deviation became less than 10 µrad (the resolution limit of the screen monitor) when it stopped.

Crystal angle offsets of C*[100] were obtained using undulator radiation and a double-crystal monochromator (DCM), as shown in Fig. 3. Only three offsets for angular motion were considered here, and any couplings between those motions were ignored for simplicity. Figs. 3(*b*)–3(*e*) show the transmitted undulator radiation spectrum where the photon loss was caused by Bragg reflections from various crystallographic planes. The 20 times lower resolution of the DCM compared with the Bragg reflection linewidth reduced the signal-to-noise ratio by 20 times and also made the absorption peaks 20 times broader, which gave a photon loss of 5% in the data. The pitch and yaw offsets were obtained by finding the center of the (004) reflection line near normal incidence while scanning each axis. The roll offset without the access of a remote motion was deduced from an iterative comparison between models and two measurements at $\psi = 0.61$ and 1.11°. The final calculations using the offset angles $(\theta, \psi, \varphi) = (0.055^\circ, 0.63^\circ, -1.43^\circ)$ were in good agreement with the experiments (see Fig. 3).

For a machine setting, electron bunches with a wide range of energy, 4–11 GeV, are used to tune a FEL energy of 2.5–15 keV while the undulator parameter remains constant ($K = 1.87$) with a period of 28 mm. The electron-bunch centroid energies for 6.95 and 8.3 keV are 7.23 and 7.90 GeV, respectively. A linear and a quadratic tapering of the 2nd–20th undulators are manually optimized to maximize FEL power

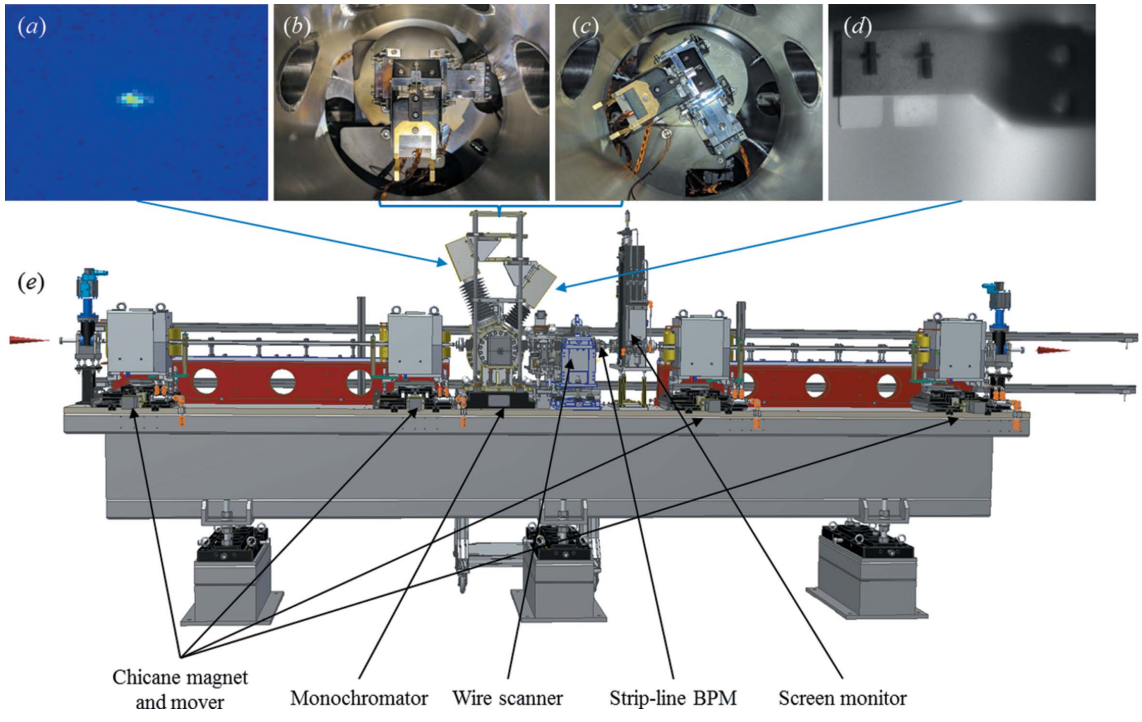

Figure 2
(*a*)–(*e*) Pictures and a 3D model of the self-seeding section. (*a*) The X-ray Bragg reflections from the diamond crystal monitored near the glancing angle of incidence, 62.5°, using a YAG:Ce scintillator. The motorized assembly at the pitch angle of (*b*) 90° and (*c*) 32°. (*d*) A surveillance camera installed to monitor the crystals for a diagnostic purpose. (*e*) A 3D model of the self-seeding section.

with a peak current of 2–3 kA. The beam parameters with a slice emittance of 0.5 mm rad (180 pC) and 0.3 mm rad (40 pC) and a slice energy spread of 2×10^{-4} are used for FEL simulations.

3. Self-seeding at low bunch charge

In April 2018, we performed the self-seeding experiment at the PAL-XFEL with a low charge of 40 pC with a repetition rate of 30 Hz at 8.3 keV. This short FEL pulse has advantages in that it can be overlapped with the first maximum of the monochromatic wake from the FBD and the electron-beam energy loss due to the wakefield effect in the undulator can be negligible. The diamond crystal in the [100] orientation with a thickness of 100 µm was inserted with the pitch angle $\theta = 56.9^\circ$ with respect to the desired photon energy.

To change the self-seeding mode, we optimized the SASE spectrum by changing the RF phase of accelerators to produce a narrow spectrum at the end of the eight-undulator segment using the single-shot spectrometer. The SASE FEL energy was measured to be 110 µJ using the *E*-loss method, while the self-seeded energy was ∼40 µJ measured using the integrated intensity from the spectrometer calibrated by the *E*-loss method.

Fig. 4(*a*) shows the average intensity of the SASE operation with a full width at half-maximum (FWHM) bandwidth of 12 eV and the self-seed FEL with a FWHM bandwidth of 0.91 eV. The peak of the average intensity for the seeding was ∼4 times higher than that of the SASE. The intensity integrated over the 1 eV bandwidth of the seeded FEL around the seeded line was 3.1 times higher than that of the SASE. The spectrum was measured by using a Si(111) single-shot spectrometer with a resolution of 0.8 eV and a wide spectral range, which could cover the full SASE spectrum.

Fig. 4(*b*) shows the single-shot spectra, where the FWHM bandwidth of seeding was 0.89 eV, which was larger than the 0.4 eV measured at the LCLS under similar experimental conditions (Amann *et al.*, 2012) because the spectral resolution of the Si(111) spectrometer was estimated to be lower than the actual bandwidth of the seeded FEL. This will also underestimate the peak spectral intensity of the seeded FEL. The FWHM bandwidth of the average intensity was close to that of the single-shot intensity, which implies that the seeding and the amplification process were stable within the spectral resolution of the spectrometer.

Figs. 4(*c*) and 4(*d*) show the measured sequence of 200 consecutive shots for the SASE operation and the self-seeded FEL, and the associated histogram of intensity integrated over a 1 eV bandwidth. The shot-to-shot jitter of the seeded FEL was over 50% because of the natural shot noise of the SASE seed, and the self-seed pulse could not reach the saturation region.

To obtain the optimal delay time of electron bunches for good overlap for the seeding, we used FBD theory (Shvyd'ko

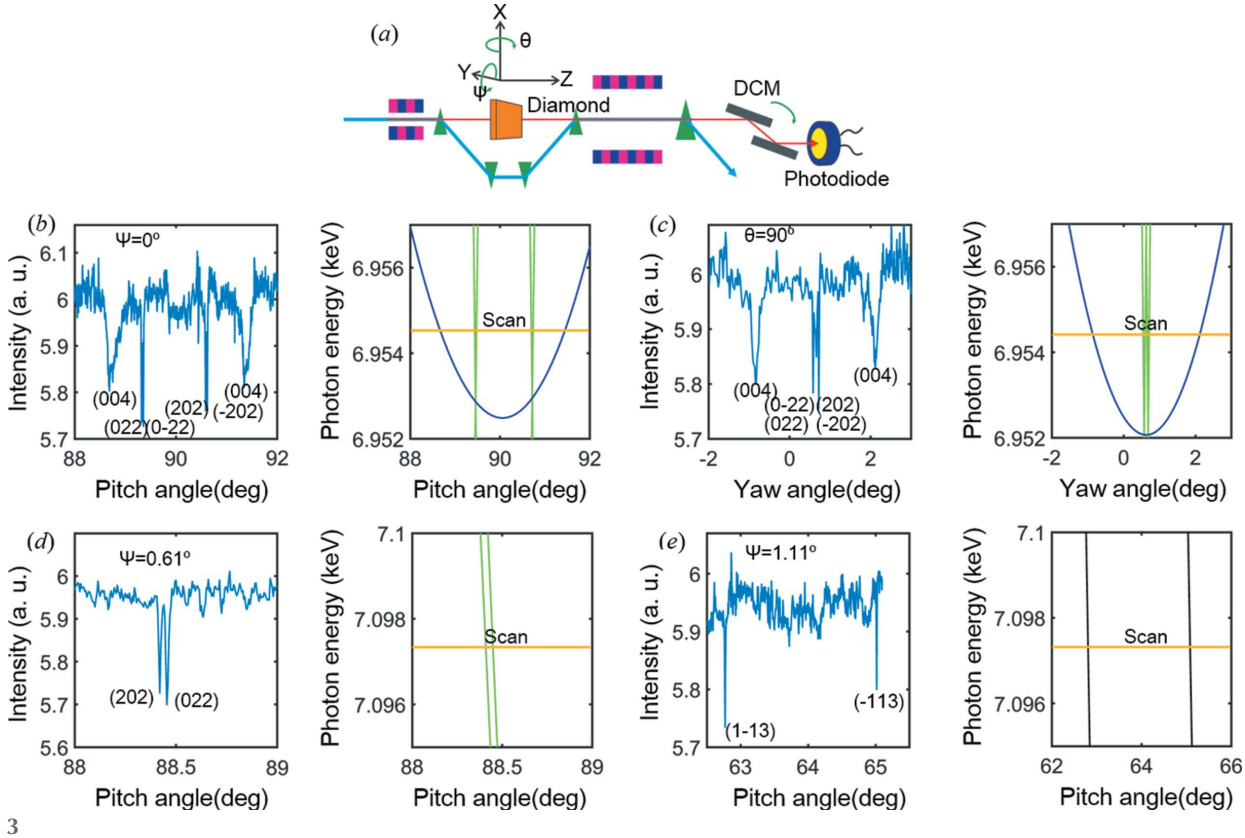

Figure 3
(*a*) Identification of the offset angles of the *C**[100] crystal based on Bragg reflection loss measurements using undulator radiation and a Si DCM. (*b*, *c*) Pitch- and yaw-angle offsets identified near normal incidence. (*d*, *e*) The roll-angle offset obtained from the comparison between the theoretical model and experiments at two different yaw angles. Three offset angles (θ, ψ, φ) = (0.055°, 0.63°, −1.43°) were obtained.

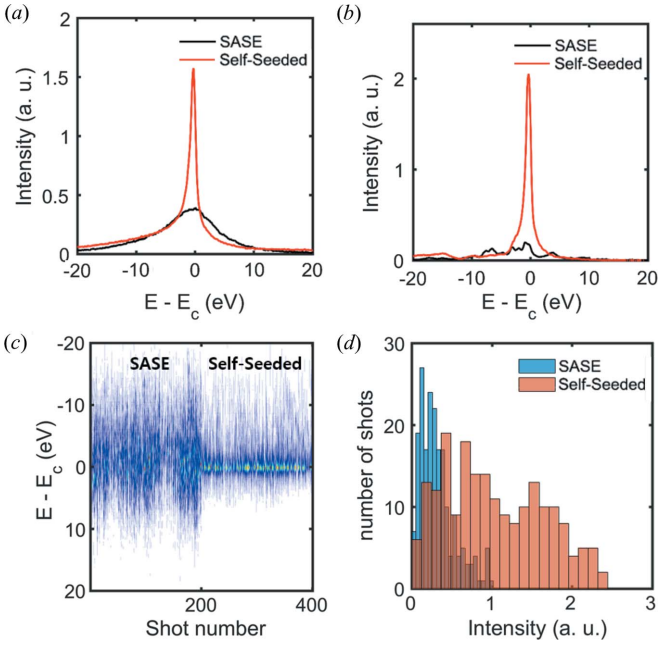

Figure 4
Short-bunch case with a low charge of 40 pC at 8.3 keV. (*a*) The average spectral intensities with an FWHM bandwidth of 12 eV (SASE) and 0.91 eV (self-seeded), respectively. (*b*) The seeded FWHM bandwidth for the typical single-shot spectra is 0.89 eV. (*c*) The 200 consecutive spectra for the SASE (#1–#200) and self-seeded FEL (#201–#400) operations. (*d*) The histograms of the integrated intensity over a 1 eV bandwidth for the SASE operation and the self-seeded FEL.

& Lindberg, 2012; Lindberg & Shvyd'ko, 2012). The FBD time response of a diamond crystal can be calculated as

$$\left|G_{00}(t)\right|^2 \propto \left(\frac{1}{2T_0}\frac{J_1\left\{(t/T_0)^{1/2}\left[1+(t/T_\mathrm{d})\right]\right\}}{(t/T_0)^{1/2}\left[1+(t/T_\mathrm{d})\right]}\right)^2, \qquad (1)$$

where $T_0 = 2\Lambda_H^2 \sin\theta/(cd)$ is the characteristic time parameter, $T_\mathrm{d} = 2d\sin\theta/\left[c\left|\sin(\theta-\eta)\right|\right]$ is the total propagation time through the crystal, d is the crystal thickness, Λ_H is the extinction length, θ is the incident angle between the X-ray and the reflecting atomic plane, η is the asymmetry angle between the crystal surface and the reflecting atomic plane, c is the speed of light, and J_1 is the Bessel function of the first kind. As a result, the first maximum of the trailing wake of the FBD time response $t_\mathrm{s} \simeq 26T_0$, its duration $t_\mathrm{d} \simeq 16T_0$, and the spectral bandwidth $\Delta E \propto 1/T_0$, are all defined by T_0. For the (400) Bragg reflection, the calculated delay of the first wake was $t_\mathrm{s} \simeq 20$ fs with Λ_H = 3.63 µm, T_0 = 0.78 fs, and $\theta = 56°$ at 8.3 keV.

Fig. 5 shows the peak intensity of the seeded FEL as a function of chicane delay for the calculated monochromatic wake from the crystal (black line) and its convolution with the SASE FEL with a bunch duration of 7 fs (FWHM) (blue line) using equation (1), which agrees well with the experimental results (red dots). One can see that the seeding occurred when the time delay was earlier than 10 fs. The optimum time delay was expected to be the first trailing maximum, $t_\mathrm{s} \simeq 20$ fs (Amann *et al.*, 2012), but we observed that the seeded FEL at

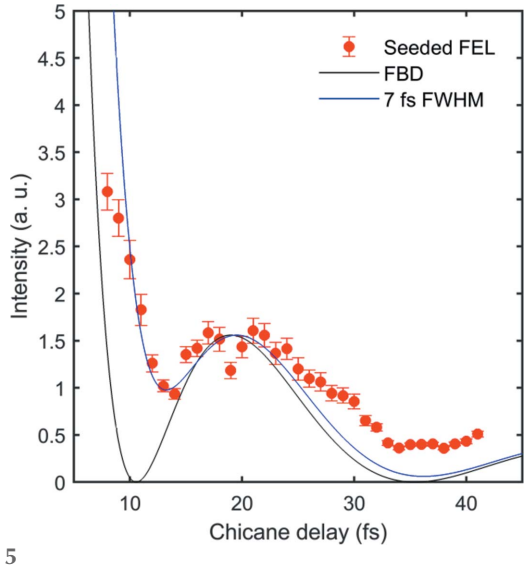

Figure 5
The peak intensity of the seeded FEL as a function of chicane delay. By using FBD theory, the blue line represents the convolution of the wake from FBD theory (black line) and the SASE FEL with an FWHM pulse duration of 7 fs, which agrees well with the experimental results (red dots).

the minimum chicane delay of 8 fs, which is in the zeroth trailing wake from the FBD, can also produce a two times higher seeded peak than that of the optimal time delay, while the FWHM bandwidth in the zeroth trailing wake increased by 10% more than one in the first trailing maximum (Yang & Shvyd'ko, 2013). This experimental evidence shows that the zeroth trailing wake of the FBD (not to be overlapped with the SASE) can be used as more efficient seeding than the maxima of the trailing wake.

4. Seeding at the nominal bunch charge

In May 2018, we carried out the self-seeding experiment for the normal-bunch mode, where the electron charge was 170–190 pC with a peak current of ∼2.5 kA at 7 keV. The nominal SASE FEL pulse had a bunch duration of 25–30 fs (FWHM) and a pulse energy of 1.2 mJ. Fig. 6 shows the FEL pulse length measurement result using the cross-correlation between the SASE pulse from the eight undulators used earlier and the electron bunch as a function of the chicane delay. The deconvoluted FEL pulse length was 29.5 fs (FWHM) assuming a Gaussian temporal profile (Ding *et al.*, 2012).

For the long electron bunch, the wakefield effect can no longer be negligible, because the electron energy is decreased in the long undulator. Thus, we slightly modified the linear undulator tapering (where the energy loss due to the wakefield effect is compensated by changing the K value to keep the resonant photon energy) for the second undulator section (U9–U20). In this case, the self-seeded FEL reached the saturation region, so we applied quadratic tapering for the last two undulator segments (U19–U20). We observed that the maximum of the seeding was produced with a chicane delay of 60 fs, where the second maximum of the trailing wake

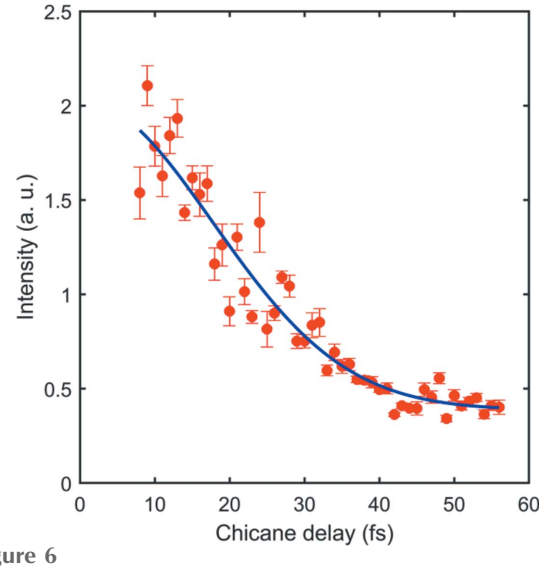

Figure 6
Measurement of SASE FEL pulse duration using the cross-correlation between the SASE FEL and the electron beam as the chicane delay changes in the self-seeding section. The FEL pulse duration was measured to be 29.5 fs (FWHM), assuming a Gaussian profile.

$t_{s2} \simeq 60$ fs was calculated using equation (1) with a T_0 of 0.86 fs for $\theta = 89.5^\circ$ and a (400) Bragg reflection. The energy of the seeded pulse (photon energy 6.95 keV) was measured to be ~430 μJ by the *E*-loss method.

Figs. 7(*a*) and 7(*b*) show the average spectral intensity with 1000 consecutive shots and the typical single-shot spectral intensity. The measured FWHM bandwidths for the average intensity are 12 eV (SASE) and 0.72 eV (seeded FEL), respectively. In a typical single-shot spectrum of the seeded FEL, the measured FWHM bandwidth was 0.64 eV, which is similar to the average one due to the very stable operation of the self-seeding system.

Figs. 7(*c*) and 7(*d*) show a sequence of 1000 consecutive shots for the SASE operation and the self-seeded FEL and their associated histograms. The seeding probability, which is defined when the peak intensity of the seeded FEL is higher than the average SASE one, was measured to be ~82%. The histogram of the integrated intensity over a 1 eV bandwidth for the seeding had a Gaussian profile, and the r.m.s. shot-to-shot jitter was 45%, which was lower than that of the short-bunch case because the seeded FEL reached the saturation region. The peak intensity of the self-seeding was ~3.5 times higher than that of the SASE, and the summed intensity of the seeding in a range of 1 eV around the seeded line was ~2.3 times higher than that of the SASE mode. One can compare the maximum flux F_m [photons pulse^{-1} (1 eV)$^{-1}$] between the long-bunch and short-bunch modes. As a result, the F_m of the long-bunch mode was an order of magnitude higher than that of the short-bunch mode.

We performed simulations using the 3D FEL code *SIMPLEX* (Tanaka, 2015) with the PAL-XFEL parameters and the crystal configuration used in the experiments for the long-bunch mode. The electron beam had a length of 6 μm (r.m.s.) and a peak current of 2400 A. The wakefield effect due to the resistive wall impedance of the undulator chamber was

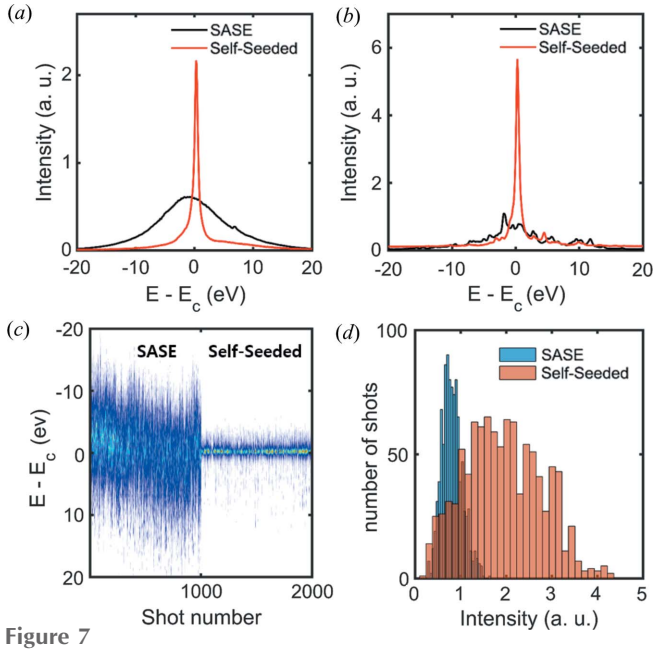

Figure 7
Long-bunch case with a nominal charge of 180 pC at 7 keV, similar to Fig. 4. (*a*) The averaged spectral intensity with an FWHM bandwidth of 12 eV for the SASE operation and 0.72 eV for the self-seeded FEL. (*b*) For the single-shot spectrum, the FWHM bandwidth for the self-seeded FEL is 0.89 eV. (*c*) The 1000 consecutive spectra for the SASE (#1–#1000) and the self-seeded FEL (#1001–#2001) operations. (*d*) The histograms of the integrated intensity over a 1 eV bandwidth for the SASE operation and the self-seeded FEL.

applied. Fig. 8(*b*) shows the evolution of the FEL energy as a function of the undulator length. The SASE energy was ~800 μJ with a pulse duration of 26 fs (FWHM). The seeded FEL was then amplified and saturated at the end of the second undulator section, where the FEL energy was ~400 μJ with a bandwidth of 0.43 eV (FWHM) using a resolution of 0.7 eV, as shown in Fig. 8(*a*). The peak of the averaged spectral intensity was ~3.5 times higher than that of the SASE, which agrees well with the experimental result. The r.m.s. shot-to-shot fluctuations of the peak intensity were 25.5% (SASE) and 51% (self-seeded), respectively. This shot-to shot fluctuation of the seeded FEL was twice that of the SASE because of the varying seeding power generated from the spiky SASE spectrum.

The PAL-XFEL has a very low shot-to-shot electron-energy jitter of 0.012%, as shown in Fig. 9. The resultant shot-to-shot fluctuation of the center energy of the SASE was measured to be 0.025%, which is two times smaller than the calculated FEL gain bandwidth $E/E_c \simeq \rho = 5 \times 10^{-4}$, where ρ is a dimensionless Pierce parameter. In addition, the effect of electron-energy jitter on the seeded FEL intensity is shown in Fig. 10. As a result, the r.m.s. electron-energy sensitivities of self-seeded intensity are 3.2×10^{-4} for the FEL simulation and 2.4×10^{-4} for the experiment, which is double our electron-energy jitter, 1.2×10^{-4}. These results have good agreement with the estimation based on the Pierce parameter. Therefore, the current electron-energy jitter does not degrade the seeded FEL intensity when maintaining the spectral overlap between SASE FEL gain and the monochromator.

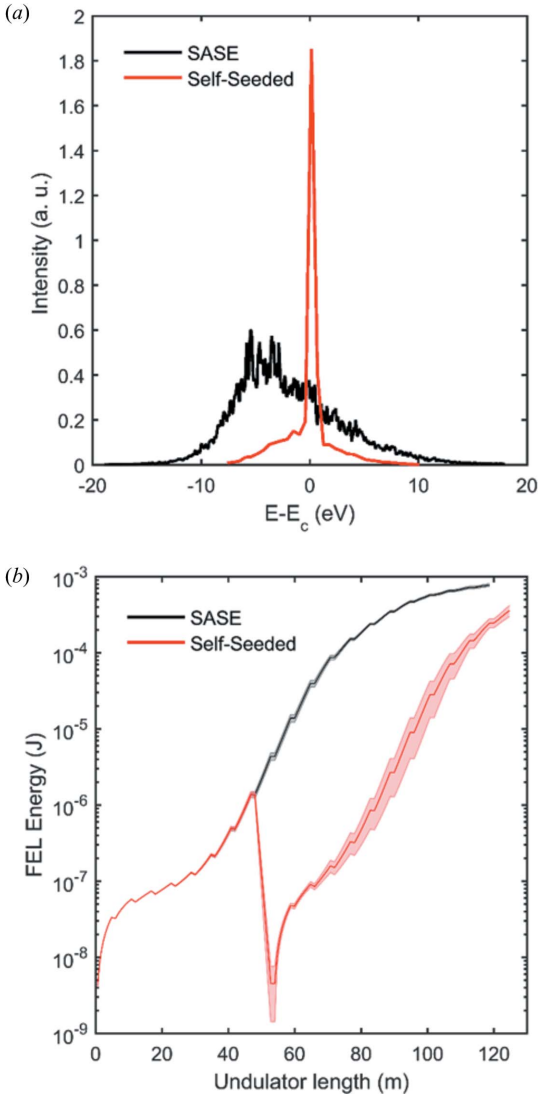

Figure 8
FEL simulation results. (*a*) Averaged intensity over 30 shots. (*b*) The FEL energy evolution for the SASE operation (black) and the self-seeded FEL (red). The shaded regions represent the r.m.s. shot-to-shot fluctuation.

5. Self-seeding using 30 μm diamond crystal

In October 2018, we used the thinner diamond crystal for the self-seeding experiment for the first time. The diamond crystal with a thickness of 30 μm in the [110] orientation can cover the spectral range from 3.3 keV to 5 keV. However, at this time, we tested this crystal at 8.3 keV using the Si(333) single-shot spectrometer with a better resolution of ∼0.2 eV. Here, we performed the self-seeding in the (220) Bragg reflection with the pitch angle $\theta = 36.5^\circ$. The electron delay was 40 fs, which was the second trailing maximum of the wake from the crystal.

According to FBD theory (Yang & Shvyd'ko, 2013), when the characteristic time T_0 decreases, the seed spectrum of the actual FBD has a double-peak structure which results in the separation between the two peaks. This separation is inversely proportional to the characteristic time T_0. For the (220) Bragg reflection, using $T_0 \simeq 0.5$ fs with $\Lambda_{220} = 1.92$ μm, the bandwidth was calculated to be $\Delta E \simeq 0.4$ eV, which was larger than that of thicker crystals (*e.g.* 100 μm in the [100] orientation). Thus, if double-color peaks are amplified in the large bandwidth, the Si(333) single-shot spectrometer can resolve these two peaks.

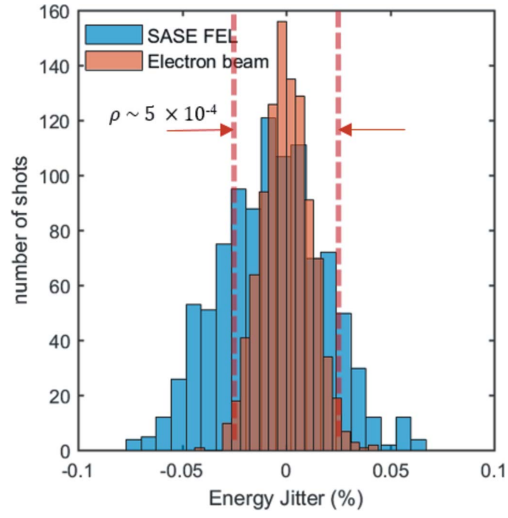

Figure 9
The shot-to-shot energy jitter distribution for the electron beam and the SASE FEL. The r.m.s. shot-to-shot fluctuations are 0.012% (electron beam) and 0.025% (SASE FEL), respectively. The dimensionless Pierce parameter ρ for PAL-XFEL with the parameters used in the experiment is calculated to be $\sim 5 \times 10^{-4}$.

Fig. 11(*a*) shows the average intensity of the FWHM bandwidth of 0.52 eV for the self-seeded FEL, in which the total bandwidth consists of two peaks. We observed that one out of the two competing peaks for the seeding was mostly amplified due to the low probability of equal-intensity double-color seeding (Yang & Shvyd'ko, 2013). As a result, over 1000 shots were observed including; 672 shots for the single-color seeding, where 310/362 shots were for the right/left peak; 235 shots for the double-color seeding; and 93 shots for no seeding as shown in Fig. 11(*c*).

When both peaks appear at the same time in the spectrum, then the peak intensity is lower than that of only single-peak amplification because the seeding power is distributed into two [see the green line in Figs. 11(*a*) and 11(*b*)]. Fig. 11(*d*) shows that the distribution of the center energy of each peak for the double-color seeding, where the separation of two peaks is ∼0.2 eV. The FWHM of the center energy for each peak is ∼0.05 eV, which shows very stable seeding operation. The FWHM bandwidth of each peak for the single-shot spectrum is ∼0.22 eV, which is the shortest bandwidth measured for the seeding experiment.

Fig. 12(*a*) represents the intensity of the seeding as a function of chicane delay from FBD theory with $T_0 \simeq 0.5$ fs. The FWHM duration of the electron beam is ∼50 fs which can be overlapped with more than one FBD wake as shown in Fig. 12(*a*). Fig. 12(*b*) shows the spectrum of the seeding radiation as covered by this long electron beam. The two peaks with an energy separation of ∼0.17 eV comes from FBD theory which results in the double-color seeding. Therefore, these experimental results agree well with FBD theory.

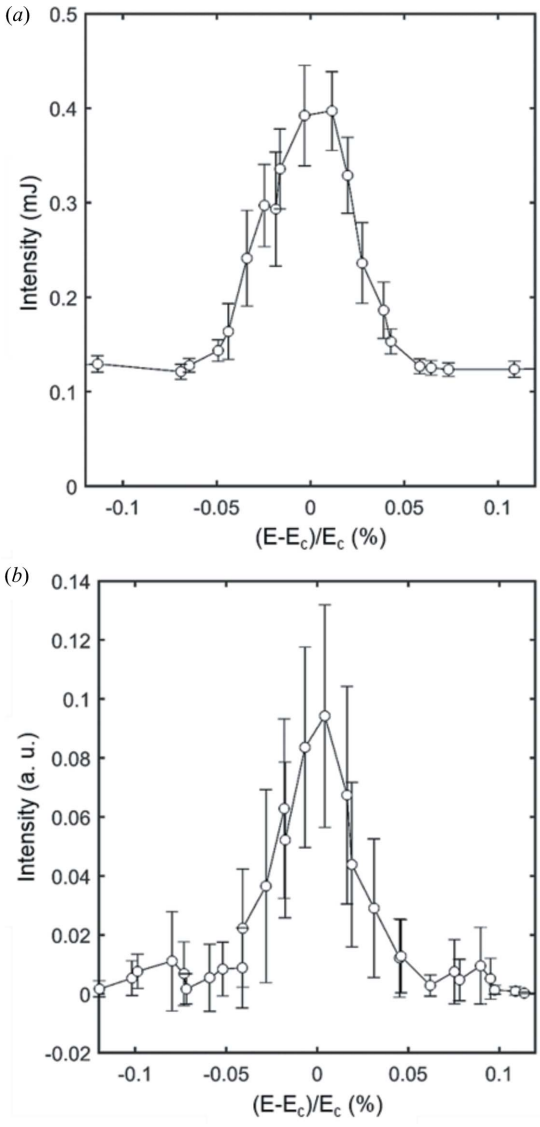

Figure 10
The self-seeded FEL intensity in FEL simulation (*a*) and the FEL intensity over a 1 eV bandwidth in experiments (*b*) as a function of the electron-energy detuning. The RMS widths for Gaussian fittings are 3.2×10^{-4} for the simulation and 2.4×10^{-4} for the experiment.

6. Summary

The PAL-XFEL hard X-ray self-seeding instrumentation has been successfully commissioned without any design flaws. To prepare the user service of the self-seeded FEL in the next year, the low bunch-charge (or short-pulse) mode and the nominal bunch-charge (or high photon-flux) mode were tested, and a more than three times improvement in spectral brightness was observed compared with the corresponding SASE mode. The 30 µm ultrathin crystal in the [110] orientation was specially added. It demonstrated that the spectral bandwidth of the seeded FEL can be as small as 0.22 eV (FWHM). The experimental and theoretical parameters related to this commissioning are summarized in Table 1. We plan to continue this commissioning below 5 keV to study the advantage of its low optical absorption. In our two-crystal system, two differently oriented crystals with [100] and [110] orientations are accommodated in a single holder and will provide more choices of T_0 in the optimization of the seeded FEL. The histogram of the integrated intensity over a 1 eV bandwidth shows that our electron-energy jitter does not greatly degrade our seeding performance.

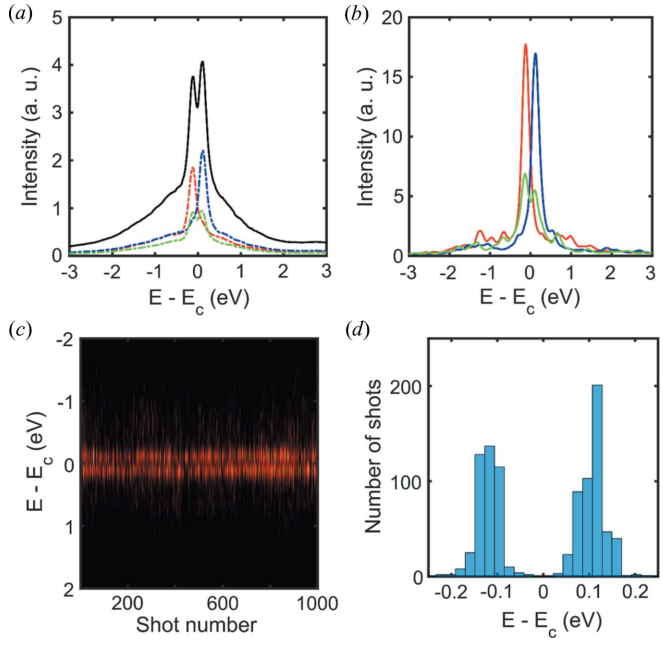

Figure 11
The thinner diamond crystal case. The diamond crystal in [110] orientation and the thickness of 30 µm are used for the (220) Bragg reflection with $\theta = 36.5^\circ$ at 8.3 keV. (*a*) The FWHM bandwidths are 0.52 eV for the average intensity of all (black solid line), 0.33 eV (0.27 eV) for average intensity of each side peak [blue (red) dotted line], and 0.43 eV for the double-color seeding (green dotted line). (*b*) The FWHM bandwidth of each single-shot spectra is 0.22 eV for the single-color peak (red, blue lines) and is 0.45 eV (green line) for the double-color seeding. (*c*) The 1000 consecutive spectra. (*d*) The histogram of the relative center position of each peak. The separation energy between the two peaks is ~0.2 eV.

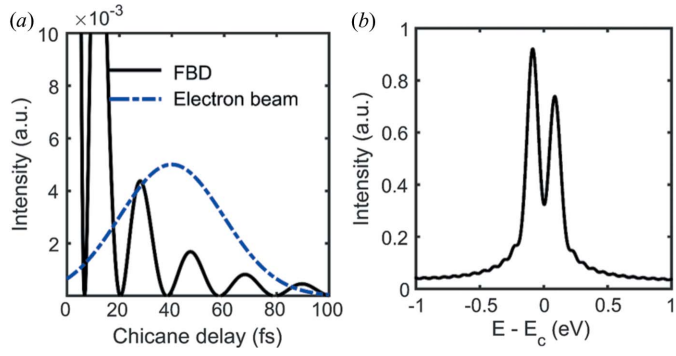

Figure 12
(*a*) Intensity of the seeding radiation as a function of the chicane delay from FBD theory for the same parameters as that of Fig. 11. The electron beam (blue dotted line) has an FWHM duration of 30 fs and a chicane delay of 40 fs. (*b*) The spectrum of the seeding radiation as covered by the electron beam that is overlapped with many wakes from FBD, which shows two separate peaks with an energy separation of 0.17 eV.

Table 1
Summarized parameters calculated from FBD theory and measured parameters from the self-seeding commissioning period.

Parameters	Short-bunch mode	Long-bunch mode	
Charge (pC)	40	180	180
FEL pulse length (fs)	7	29.5	29.5
Crystal thickness d (μm)	100	100	30
E_c (keV)	8.3	7	8.3
Θ (°)	56.6	89.5	36.5
FBD theory			
H (hkl)	400	400	220
Λ_H (μm)	3.63	3.63	1.92
T_0 (fs)	0.78	0.86	0.5
t_d (fs)	12.5	13.8	8
t_s (fs)	20.3	22.4	13
ΔE (eV)	0.287	0.24	0.40
Experiment			
Chicane delay (fs)	20	60	40
ΔE (eV)	0.89†	0.64†	0.56‡

† Si (111) spectrometer used. ‡ Si (333) spectrometer used.

Acknowledgements

The authors would like to thank Dr Franz-Josef Decker, Dr Alberto Lutman, Dr Svitozar Serkerz, Dr Gianluca Geloni and Dr Shan Liu for helpful discussions.

Funding information

This research has been supported by the Ministry of Science and ICT of Korea and partly by the Basic Science Research Program (Grant No. 2017R1A2B4007274) through the National Research Foundation of Korea (NRF) funded by the Ministry of Science and ICT of Korea.

References

Amann, J., Berg, W., Blank, V., Decker, F., Ding, Y., Emma, P., Feng, Y., Frisch, J., Fritz, D., Hastings, J., Huang, Z., Krzywinski, J., Lindberg, R., Loos, H., Lutman, A., Nuhn, H., Ratner, D., Rzepiela, J., Shu, D., Shvyd'ko, Y., Spampinati, S., Stoupin, S., Terentyev, S., Trakhtenberg, E., Walz, D., Welch, J., Wu, J., Zholents, A. & Zhu, D. (2012). *Nat. Photon.* **6**, 693–698.

Ding, Y., Decker, F. J., Emma, P., Feng, C., Field, C., Frisch, J., Huang, Z., Krzywinski, J., Loos, H., Welch, J., Wu, J. & Zhou, F. (2012). *Phys. Rev. Lett.* **109**, 254802.

Geloni, G., Kocharyan, V. & Saldin, E. (2011). *J. Mod. Opt.* **58**, 1391–1403.

Gutt, C., Wochner, P., Fischer, B., Conrad, H., Castro-Colin, M., Lee, S., Lehmkühler, F., Steinke, I., Sprung, M., Roseker, W., Zhu, D., Lemke, H., Bogle, S., Fuoss, P. H., Stephenson, G. B., Cammarata, M., Fritz, D. M., Robert, A. & Grübel, G. (2012). *Phys. Rev. Lett.* **108**, 024801.

Huang, Z. & Kim, K.-J. (2007). *Phys. Rev. ST Accel. Beams*, **10**, 034801.

Kang, H. S., Min, C. K., Heo, H., Kim, C., Yang, H., Kim, G., Nam, I., Baek, S. Y., Choi, H. J., Mun, G., Park, B. R., Suh, Y. J., Shin, D. C., Hu, J., Hong, J., Jung, S., Kim, S. H., Kim, K., Na, D., Park, S. S., Park, Y. J., Han, J. H., Jung, Y. G., Jeong, S. H., Lee, H. G., Lee, S., Lee, S., Lee, W. W., Oh, B., Suh, H. S., Parc, Y. W., Park, S. J., Kim, M. H., Jung, N. S., Kim, Y. C., Lee, M. S., Lee, B. H., Sung, C. W., Mok, I. S., Yang, J. M., Lee, C. S., Shin, H., Kim, J. H., Kim, Y., Lee, J. H., Park, S. Y., Kim, J., Park, J., Eom, I., Rah, S., Kim, S., Nam, K. H., Park, J., Park, J., Kim, S., Kwon, S., Park, S. H., Kim, K. S., Hyun, H., Kim, S. N., Kim, S., Hwang, S. M., Kim, M. J., Lim, C. Y., Yu, C. J., Kim, B. S., Kang, T. H., Kim, K. W., Kim, S. H., Lee, H. S., Lee, H. S., Park, K. H., Koo, T. Y., Kim, D. E. & Ko, I. S. (2017). *Nat. Photon.* **11**, 708–713.

Lindberg, R. & Shvyd'ko, Y. V. (2012). *Phys. Rev. ST Accel. Beams*, **15**, 050706.

Saldin, E. L., Schneidmiller, E. A., Shvyd'ko, Y. V. & Yurkov, M. V. (2001). *Nucl. Instrum. Methods Phys. Res. A*, **475**, 357–362.

Shvyd'ko, Y. V., Anton, J. W. J., Kearney, S. P., Kim, K. -J., Kolodziej, T., Shu, D., Blank, V. D., Terentiev, S., Kang, H. -S., Min, C. -K., Oh, B. G. & Vodnala, P.(2017). *Proceedings of the 38th International Free-Electron Laser Conference (FEL2017)*, 20–25 August 2017, Santa Fe, New Mexico, USA, pp. 29–33. MOP001.

Shvyd'ko, Y. V. & Lindberg, R. (2012). *Phys. Rev. ST Accel. Beams*, **15**, 100702.

Tanaka, T. (2015). *J. Synchrotron Rad.* **22**, 1319–1326.

Yang, X. & Shvyd'ko, Y. V. (2013). *Phys. Rev. ST Accel. Beams*, **16**, 120701.

Zhu, D. L., Cammarata, M., Feldkamp, J. M., Fritz, D. M., Hastings, J. B., Lee, S., Lemke, H. T., Robert, A., Turner, J. L. & Feng, Y. P. (2012). *Appl. Phys. Lett.* **101**, 034103.